Journal of Hazardous Materials 500 (2025) 140502

Contents lists available at ScienceDirect

Journal of Hazardous Materials

journal homepage: www.elsevier.com/locate/jhazmat

Transport and retention mechanism of microplastics in saturated porous media: Dominance of layer sequence and modulation by solution chemistry

Didi Li [a], Shihao Zhen [a], Yuzhe Qin [a], Zhimin Ao [b,*]

[a] Guangdong Key Laboratory of Environmental Catalysis and Health Risk Control, Guangdong-Hong Kong-Macao Joint Laboratory for Contaminants Exposure and Health, School of Environmental Science and Engineering, Guangdong University of Technology, Guangzhou 510006, China
[b] Guangdong Provincial Key Laboratory of Wastewater Information Analysis and Early Warning, School of Technology for Sustainability, Advanced Interdisciplinary Institute of Environment and Ecology, Beijing Normal University, Zhuhai 519087, China

HIGHLIGHTS

- Effects of layered structure and solution chemistry on MPs transport are studied.
- MPs mobility in layered media follows C-F > C-F-C > F-C.
- Layer sequence controls MP retention in saturated porous media.
- Solution chemistry (IS, cation, pH) modulates MP transport in C-F structure.
- Fine layers act as key retention hotspots across varied conditions.

GRAPHICAL ABSTRACT

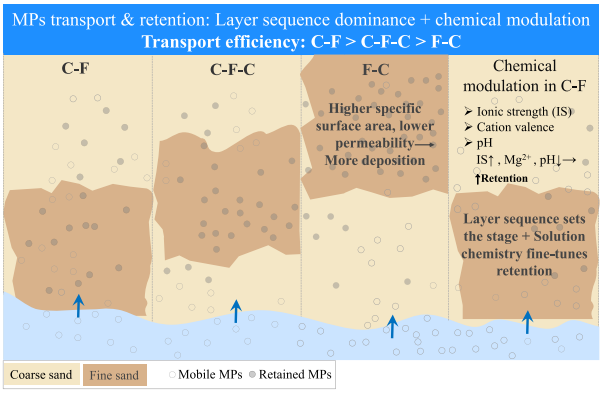

ARTICLE INFO

Keywords:
Microplastics transport
Layered porous media
Deposition kinetics
Solution chemistry
DLVO theory

ABSTRACT

Microplastics (MPs) pose significant environmental risks due to their persistence and potential to contaminate soil and groundwater. This study investigated the transport and retention of MPs in saturated porous media, focusing on how the sequence of layered sand structures (Coarse-Fine: C-F; Coarse-Fine-Coarse: C-F-C; Fine-Coarse: F-C) controlled MP fate, and how this physical framework was modulated by solution chemistry. Controlled column experiments revealed that the physical structure, specifically the layer sequence, was the primary driver of MP retention. This "layer sequence effect" predominantly governed MP mobility, with transport efficiency decreasing in the order: C-F > C-F-C > F-C. When the fine layer was positioned farthest from the inlet, its higher specific surface area and lower permeability more readily facilitated MP deposition. The influence of solution chemistry (ionic strength: 1–30 mM; cation valence: Na^{+} *vs.* Mg^{2+}; pH: 5–9) was systematically examined within the C-F structure. Increased ionic strength and the presence of Mg^{2+} enhanced MP retention, while higher pH (*e.g.*, 9) promoted MP transport. Nevertheless, the significantly higher retention in the fine sand layer remained the dominant pattern across all chemical conditions. These findings underscore that the geological framework sets the stage for MP transport, while solution chemistry modulates the attachment efficiency within that framework. This work establishes a mechanistic baseline under controlled conditions and

* Corresponding author.
E-mail address: zhimin.ao@bnu.edu.cn (Z. Ao).

https://doi.org/10.1016/j.jhazmat.2025.140502
Received 15 July 2025; Received in revised form 10 November 2025; Accepted 14 November 2025
Available online 15 November 2025

demonstrates the necessity of incorporating stratigraphic architecture, especially layer sequence, into predictive models and risk assessments for MP contamination.

1. Introduction

Microplastics (MPs) are a pervasive environmental contaminant, increasingly detected in terrestrial and aquatic ecosystems [1,2]. Their entry into soils occurs through multiple pathways, including flooding, irrigation, atmospheric deposition, and improper waste disposal [3–5]. Due to their chemical stability, MPs can persist in soils for decades, undergoing progressive fragmentation and leading to their gradual accumulation [6]. A critical environmental concern is their strong potential for vertical transport through the soil profile, which poses a direct threat of groundwater contamination [7]. This migration can be significantly accelerated by natural hydrological processes, particularly cyclic groundwater table fluctuations during aquifer recharge and discharge, which can remobilize retained MPs and facilitate their spread through subsurface environments [8]. Given the direct link between MP contamination and human health risks, including inflammation, oxidative stress, and metabolic disorders [9,10], understanding the mechanisms governing MP migration in soils is essential for predicting their distribution and mitigating potential hazards.

In saturated soils, solution chemistry properties such as ionic strength (IS), cation valence, and pH play a crucial role in the transport and retention of MPs [11]. Studies have shown that MPs generally exhibit greater mobility in porous media under conditions of lower IS, higher pH, and in the presence of monovalent cations (*e.g.*, Na^{+}) [12–14]. As IS increases, the electrostatic double layer is compressed, lowering the primary energy barrier between MPs and sand particles, allowing van der Waals attraction to dominate [15,16]. According to the Derjaguin-Landau-Verwey-Overbeek (DLVO) theory, these changes enhance MP capture and reduces their mobility in porous media [5,14, 17]. Similarly, a decrease in pH makes the zeta potential of MPs less negative or even positive, weakening electrostatic repulsion and enhancing deposition of MPs onto sand particles, thereby also promoting their retention [13,14,18,19]. The mobility of MPs also reduces with increasing cation valence [14]. Divalent cations (*e.g.*, Mg^{2+}, Ca^{2+}) and trivalent cations (*e.g.*, Al^{3+}) more effectively screen the negative surface charge of MPs, significantly lowering the energy barrier and reducing the mobility of MPs compared to monovalent cations (*e.g.*, Na^{+}) [12,13, 20,21].

Apart from solution chemistry, porous media properties such as grain size also significantly impact the transport and retention of MPs [22]. Generally, a decrease in grain size reduces MP mobility and enhances retention [17,23,24]. This is because finer-grained media, with their lower permeability, reduced porosity, and larger specific surface area, feature narrower pore throats and more deposition sites, which collectively enhance MP retention [13,14]. Solution chemistry further modulates these dynamics by altering the surface charge properties of both MPs and the media. The combined effects of solution chemistry and grain size on MP transport are complex and often nonlinear. For instance, under high IS conditions which already favored MP deposition, smaller grain sizes significantly reduced MP mobility. However, increased IS contributed little to further retention beyond that caused by reduced grain size [17].

It is worth noting that real-world soil systems are commonly stratified, with each layer having distinct grain sizes. These layered structures differ in permeability, porosity, and surface roughness, which can directly affect the transport and distribution of MPs within the layers. For instance, abrupt contrasts in permeability between adjacent layers can significantly distort flow fields, often inducing preferential flow paths, trapping MPs at layer interfaces, or altering vertical migration rates, phenomena that are absent in homogeneous single-layer systems. Furthermore, the aggregation of MPs caused by solution chemistry can alter the pore size and distribution in porous media, potentially plugging large pores. This could reduce porosity and may in turn affect the transport of MPs in the porous media [25]. However, a critical knowledge gap persists. Existing research on porous media has often treated grain size as a homogeneous property or compared different types of media in isolation. There is a distinct lack of studies focused explicitly on how the specific sequence and arrangement of layers control MP fate. The transport mechanisms of MPs across the heterogeneous interfaces of saturated layered structures, which more accurately represent natural subsurface environments, remain poorly understood and severely under-researched. This lack of knowledge fundamentally limits our ability to accurately predict the fate, spread, and long-term retention of MPs in realistic field conditions.

To bridge this gap, this study integrated transparent column experiments featuring diverse layered porous media configurations and HYDRUS-1D simulations. The unique contributions and innovative aspects of this work are threefold: First, we systematically constructed three typical stratified systems (Coarse-Fine: C-F; Coarse-Fine-Coarse: C-F-C; Fine-Coarse: F-C) to explicitly characterize MP transport and retention behaviors across heterogeneous interfaces, a scenario largely unexplored in previous work. Second, we selected a representative layered structure to investigate the synergistic effects of key solution chemistry properties, including ionic strength (IS, adjusted to 1–30 mM using NaCl and $MgCl_2$ as the dominant divalent cation to preclude complications from Ca^{2+}-phosphate precipitation), cation valence (monovalent *vs*. divalent), and pH (5–9), on MP dynamics in a stratified environment. Finally, by linking experimental data with modeling results, this study elucidated how stratification and solution chemistry control MP migration, providing a comprehensive scientific basis for risk assessment and management of MP contamination in complex subsurface environments.

2. Materials and methods

2.1. Materials and preparatory work

The migration of MPs in saturated layered systems was simulated using fine sand and coarse sand (supplied by Henan Yilong Environmental Protection Technology Co., Ltd). These sands were selected based on their grain size distribution to create layers with significantly different hydraulic conductivities, thereby enabling a systematic investigation of the effect of physical heterogeneity on MP transport. The grain sizes of the coarse sand (0.5–1.0 mm) and fine sand (0.1–0.3 mm) correspond to the “coarse sand” and “fine sand” categories, respectively, as defined by the United States Department of Agriculture (USDA) soil texture classification system for soil separates, making them relevant models for common subsurface environments like sandy aquifers and sediments. Key properties of the sands, including grain size, bulk density, porosity, and permeability coefficient, are shown in Table 1. The permeability coefficient of the sands was measured by the classic Darcy experiment, and the porosity was measured by the liquid saturation method.

Polystyrene (PS) particles with a nominal size of 1 μm were selected

Table 1
Properties of the fine and coarse sands.

Sand	Diameter (mm)	Bulk density (g/cm^3)	Porosity (%)	Permeability coefficient (cm/s)
Coarse	0.5–1.0	1.9	41.7	2.83×10^{-2}
Fine	0.1–0.3	1.8	37.9	2.24×10^{-3}

as model MPs due to their widespread industrial use and environmental relevance [26]. These particles were obtained as a 25 mg/mL aqueous stock suspension from Jiangsu Zhichuan Technology Co., Ltd. Characterization of the particle size distribution (Fig. S1) confirmed that the majority of the MP particles (over 54 %) were close to the nominal size of 1 μm, with deviations of less than ±0.047 μm. This tight size distribution helped to ensure more consistent and controlled experimental conditions for studying the MP transport.

The coarse sand and fine sand were respectively screened using sieves of 20–30 mesh and 60–70 mesh. Then they were ultrasonically cleaned using a 100SD-5 ultrasonic cleaner (JIILMAIY, Co., Ltd., Huizhou, China) for 20 min to remove stubborn stains on the sand surfaces. Notably, the sands were soaked separately in hydrochloric acid solution (1 M) and NaOH solution (1 M) for 8 h each, followed by rinsing with deionized (DI) water until neutral. This rigorous cleaning procedure was employed to remove potential impurity ions and organic coatings, thereby standardizing the surface chemistry of the sands. This control was essential to minimize variability in intrinsic adsorption properties and to allow us to focus clearly on the effects of macroscopic physical heterogeneity (*i.e.*, the layered structure and the position of the fine sand layer) and the solution chemistry. The cleaned sands were then placed in an electric drying oven (model DHG-9145A from YIHENG, Co., Ltd., Shanghai, China) and dried at 50 ℃ for 48 h before being stored in dry conditions for subsequent use. To prepare the working suspension, 100 μL of the stock MP suspension was diluted with background solutions (NaCl or $MgCl_2$ at the specified concentration in Table 2) to a final 50 mL, resulting in a final MP concentration of 50 mg/L. The suspension was then ultrasonically treated for 10 min using the ultrasonic cleaner to ensure even dispersion and to minimize particle aggregation.

2.2. Experimental setup

The schematic diagram of the experimental device is shown in Fig. 1. Initially, sand was carefully filled into a specifically designed acrylic column, which had an inner diameter of 1 cm and a height of 10 cm. During the filling procedure, after each addition of 0.5 cm height of sand, the column was gently tapped 10 times with a rubber hammer to compact the sand layer and ensure structural integrity. To prevent sand leakage from both the bottom and top of the column, 100-mesh screens were securely fitted at these openings.

In order to explore the transport and retention mechanisms of MPs within layered systems, three distinct layered configurations were constructed (Fig. 1): Coarse-Fine (C-F), consisting of a 5 cm coarse sand layer over a 5 cm fine sand layer; Coarse-Fine-Coarse (C-F-C), featuring a 2.5 cm coarse layer at the top, a 5 cm fine layer in the middle, and a 2.5 cm coarse layer at the bottom; and Fine-Coarse (F-C), comprising a 5 cm fine layer over a 5 cm coarse layer. For comparison, single-layer systems consisting solely of coarse sand (C) and fine sand (F) were also investigated. All experiments investigating the effect of layer configuration (*i.e.*, systems C, F, C-F, C-F-C, F-C) were conducted under identical background solution conditions: 1 mM NaCl at pH 7 (Table 2).

Table 2
Case setting considered in this study.

Case	Structure	IS (mM)	Cation	pH
1	C	1	Na^+	7
2	F	1	Na^+	7
3	C-F	1	Na^+	7
4	C-F-C	1	Na^+	7
5	F-C	1	Na^+	7
6	C-F	10	Na^+	7
7	C-F	30	Na^+	7
8	C-F	1	Mg^{2+}	7
9	C-F	30	Mg^{2+}	7
10	C-F	1	Na^+	5
11	C-F	1	Na^+	9

It should be noted that no physical demarcation, such as a mesh or screen, was employed at the interfaces between sand layers in our experiments. This intentional design choice was made to better simulate naturally occurring gradational interfaces, which are more representative of real-world subsurface conditions than artificially sharp boundaries. Furthermore, the omission of a barrier prevents the introduction of experimental artifacts, such as preferential flow, particle clogging, or unrepresentative filtration, which could alter solute transport and retention mechanisms. Instead, we relied on controlled packing methods and low hydraulic gradients to maintain interface stability. Sand was deposited in 0.5 cm increment, each was gently compacted to minimize disturbance and ensure uniformity. The column was slowly saturated from the bottom upward, and experiments were conducted under stable low-flow conditions (1.0 ± 0.2 mL/min). This flow rate maintained hydraulic gradients well below the critical threshold for particle mobilization, thereby preserving interface stability throughout the experiments.

To investigate the effects of solution chemistry on MP transport and retention, the C-F layered configuration was selected as a representative system. In this system, three IS levels (1, 10, and 30 mM) using NaCl solutions were first compared. To isolate the specific effect of cation valence (Na^+ *vs.* Mg^{2+}) on MP transport, solutions were prepared at matched IS. Based on the definition $IS = \frac{1}{2}\sum c_i \cdot z_i^2$ (c_i is the ion concentration, and z_i is its valance), a divalent Mg^{2+} ion contributes four times more to IS than a monovalent Na^+ ion at an equivalent concentration. Therefore, correspondingly lower concentrations of $MgCl_2$ (0.33 mM or 10 mM) were used to achieve the same IS as the NaCl solutions (1 mM or 30 mM, respectively). This precise matching ensures that any observed differences in MP behavior are unequivocally attributed to cation valence rather than differences in the overall ionic environment. The pH of the NaCl solutions was also adjusted to three different values (5, 7, and 9) using HCl or NaOH. In each solution, the zeta potentials of MPs and sand particles were measured separately using a Zeta sizer Nano ZS analyzer (Malvern Instruments, Ltd., Worcestershire, UK) through electrophoretic mobility analysis at an applied voltage of 50 V (Table S1). For the layered structures, volume-averaged physicochemical properties such as mean zeta potential were derived from the overall composition (50 % coarse sand and 50 % fine sand by volume for all three layered structures). To ensure reproducibility, all experimental cases, including different layer configurations and solution chemistry variations, were conducted in three independent trials. The data points and error bars as shown in the resulting figures (e.g., Fig. 2 and Fig. 3) were calculated from these triplicate measurements. The small relative errors (generally below 10 %) observed confirm the excellent reproducibility of the packing method and experimental measurements.

A peristaltic pump (YX-LP01-P100, Yanxiao Technology Co., Ltd., Shanghai, China) was used to pump the background solution and MPs suspension into the sand column at a flow rate of 1.0 ± 0.2 mL/min. First, the background solution was pumped through the column for 3 h to achieve pre-equilibration. This step aimed to establish stable initial state hydrodynamic conditions, remove residual air and soluble impurities, and guarantee the accuracy of subsequent experimental data. The MPs suspension was then pumped for 40 min, which corresponded to approximately 13.3 pore volumes (PV, see **Text S1** for calculation and approximation). Under these experimental conditions (1 μm MPs, low salinity), no significant aggregation or settling was observed, and thus no additional anti-sedimentation measures were employed. Then the background solution was pumping for 35 min (*i.e.*, ~11.7 PV) to simulate flushing of contaminated soils by rising clean groundwater. Throughout the MPs suspension pumping and subsequent background solution pumping (total: 75 min, 25.0 PV), effluent at the column outlet was collected sequentially. The outflow was continuously diverted into a fresh 10 mL tube every 3 min (representing approximately 1.0 PV per tube). A total of 25 test tubes were used, covering the entire process. Prior to absorbance measurement, each collected sample was

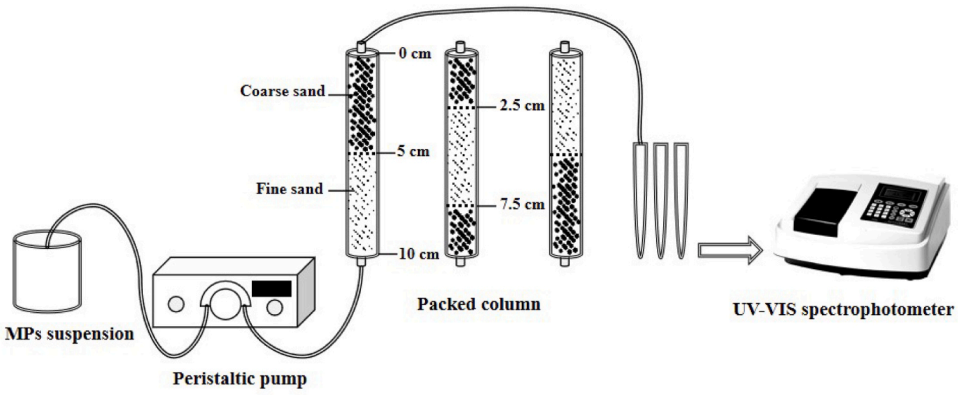

Fig. 1. The schematic diagram of the experimental device.

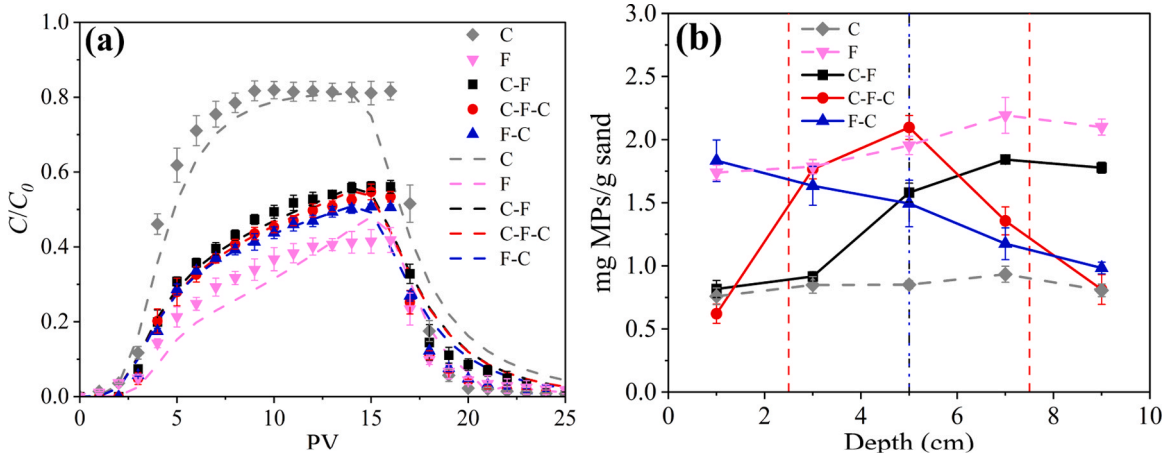

Fig. 2. Impact of sand structures on transport and retention of MPs in saturated porous media: (a) breakthrough curves (symbols: experimental data; dashed lines: fitting curves); (b) retention profiles (red vertical dashed lines: layered interfaces for the C-F-C structure; black and blue dashed lines: layered interfaces for C-F and F-C structures).

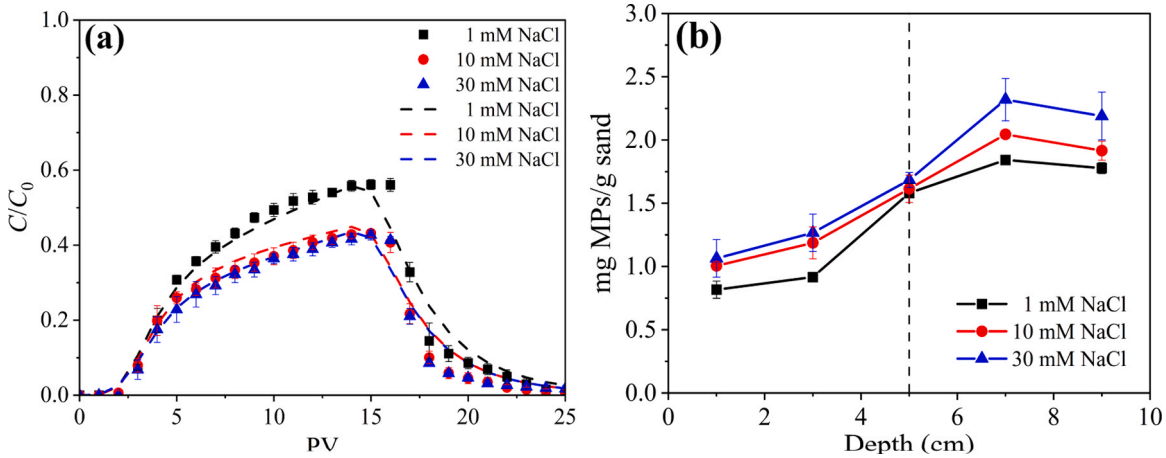

Fig. 3. Impact of different ionic strengths of Na^+ solutions (1, 10, and 30 mM) on transport and retention of MPs in the C-F structure: **(a)** breakthrough curves (symbols: experimental data; dashed lines: fitting curves); **(b)** retention profiles (black dashed line: layered interface for the C-F structure).

thoroughly mixed. The absorbance of the samples was measured at 251 nm using a UV–VIS spectrophotometer (UV-756S, Lengguang Technology Co., Ltd., Shanghai, China). This wavelength was identified as the maximum absorption wavelength for the MPs suspension through a preliminary full-wavelength scan (Fig. S2). The relationship between absorbance and MPs concentration was established using a standard calibration curve (Fig. S3).

After the leaching experiment, the sand column was slowly extruded and sectioned into five horizontal slices. The mass of each sand slice was measured using an analytical balance (YHM-6001, Yingheng Electronics Technology Co., Ltd., Huizhou, China). Each sand slice was then transferred into a 50 mL sample bottle containing 30 mL DI water to

resuspend the retained MPs. The absorbance of the resulting MPs suspension in DI water was measured using the UV–VIS spectrophotometer. The mass of MPs in each suspension was calculated based on the measured absorbance and the known volume of DI water, utilizing the established calibration curve. These mass values were then used to construct retention profiles (RPs) that quantify MPs distribution at different depths within the column. To complement these macroscopic results (breakthrough curves and retention profiles) with visual evidence, the morphology of MPs adhering to sand surfaces was examined using scanning electron microscopy (SEM) (SU8220, Hitachi, Japan). The C-F-C structure was selected for this detailed visualization as it represents the most complex and information-rich configuration, incorporating both coarse-fine and fine-coarse interfaces. This dual-interface architecture simulates the heterogeneous layering prevalent in natural porous media such as soils and aquifers. While the effluent and retention data quantitatively characterized the behavior of all five structures, the SEM analysis of the C-F-C column (Fig. S4) provides a mechanistic understanding applicable to the others, particularly regarding the role of fine sand layers and interfacial dynamics.

2.3. Mathematical modeling and DLVO calculation

HYDRUS-1D is a widely used numerical software for simulating one-dimensional transport of water, solutes, heat, and colloids in variably saturated porous media. Its application to the transport of MPs leverages the two-site kinetic retention model to describe mass transfer between aqueous and solid phases [20,27]:

$$\frac{\partial(\theta C)}{\partial t}+\rho_b\frac{\partial(S_1)}{\partial t}+\rho_b\frac{\partial(S_2)}{\partial t}=\frac{\partial}{\partial z}\left(\theta D\frac{\partial C}{\partial z}\right)-\frac{\partial qC}{\partial z} \quad (1)$$

where θ represents the volumetric water content; C is the concentration of MPs in solution; t is time; ρ_b is the bulk density of the porous medium; S_1 and S_2 are the concentrations of MPs adsorbed onto the solid phase (mass of MPs per mass of solid) for kinetic Site 1 and Site 2, respectively; z is coordinate in the vertical flow direction; D is the hydrodynamic dispersion coefficient; and q is the Darcy velocity. The dispersion coefficient (D) was determined via conservative tracer tests using 20 mg/L methyl orange (**Text S2** and Fig. S5).

The two-site model assumed the presence of two types of retention sites on the surface of the porous medium, *i.e.*, Site 1, exhibiting kinetically reversible attachment (hereafter referred to as "reversible"), and Site 2, exhibiting kinetically limited reversibility (hereafter referred to as "irreversible") [27]:

$$\rho_b\frac{\partial S_1}{\partial t}=\theta k_1 C-k_{1d}\rho_b S_1 \quad (2)$$

$$\rho_b\frac{\partial S_2}{\partial t}=\theta k_2\psi C \quad (3)$$

where k_1 and k_2 are the first-order attachment coefficients for Site 1 and Site 2, respectively; k_{1d} is the first-order detachment coefficient for Site 1; ψ is the colloidal retention function accounting for site limitation (blocking), defined as:

$$\psi=1-\frac{S_2}{S_{2,\max}} \quad (4)$$

where $S_{2,\max}$ is the maximum retention capacity at Site 2. Notably, Eq. (3) includes no detachment term, reflecting the irreversible retention assumption for Site 2. It is important to note that the assignment of "reversible" and "irreversible" is a relative conceptualization within the model framework, where "irreversible" denotes a state with a significantly lower probability of detachment under the prevailing experimental conditions, rather than an absolute state.

To elucidate the underlying mechanisms of MP retention and support the conceptualization of the reversible (Site 1) and irreversible (Site 2) deposition sites, interaction energies between MPs and sand were calculated using the classical DLVO theory. This theory was employed not as a predictive tool but served primarily as a conceptual baseline, aiming to establish a scenario based on volume-averaged properties. The discrepancy between its predictions and the experimental observations was then used to qualitatively highlight the significance of non-DLVO factors. Within this framework, the total interaction energy (E_{TOTAL}) is the sum of van der Waals attraction (E_{VDW}) and the electrostatic double layer repulsion (E_{EDL}): $E_{TOTAL}= E_{VDW} + E_{EDL}$. The calculations of the interaction energies under different conditions are provided in **Text S3**.

3. Results and discussion

3.1. Transport behavior of MPs in layered structures

Fig. 2a shows the breakthrough curves (BTCs) for MPs in different sand structures, where symbols denote experimental data and dashed lines represent fitting results from HYDRUS-1D simulations. In the context of BTCs, C/C_0 refers to the ratio of the solute effluent concentration (C) at the outlet to the initial influent concentration (C_0) at the inlet. The BTCs in the single-layer C structure showed the fastest arrival and highest plateau of MP breakthrough, while the single-layer F structure had the slowest rise and lowest maximum effluent concentration. The BTCs of the three layered structures exhibited breakthrough behaviors intermediate between those of the two single-layer structures. Among these layered structures, the BTCs exhibited similar shapes but distinct maximum C/C_0 values, following the order: C-F > C-F-C > F-C. This indicated varying extents of MP breakthrough among the layered structures. As shown in Table S2, the maximum effluent concentration (*MEC*) of MPs in the C structure reached 0.813, and the total mass percentage of MPs recovered from the effluent (M_{eff}) reached 73.4 %. In contrast, in the F structure, the *MEC* and M_{eff} of MPs were significantly lower, at 0.389 and 31.3 %, respectively. Among the three layered structures, the C-F structure showed the highest *MEC* and M_{eff} at 0.561 and 51.4 %, while the F-C structure had the lowest at 0.508 and 45.1 %, with C-F-C falling in between. These results suggested that the C-F structure exhibited the highest mobility of MPs among the three layered structures.

The tailing observed in the BTCs during the flushing phase (after 13.3 PV) indicated a slow release of previously retained MPs back into the aqueous phase. This phenomenon is attributed to reversible attachment-detachment processes. To quantitatively validate this mechanism, the experimental BTC data were fitted using HYDRUS-1D, applying its two-site kinetic retention model. The simulations closely matched the experimental data ($R^2 > 0.95$, Table S2), confirming the applicability of the model and its two-site mechanism. The fitting parameters provide insight into the deposition kinetics governing MP transport. For reversible deposition sites (Site 1), both the attachment coefficient (k_1) and detachment coefficient (k_{1d}) across different structures (Cases 1–5) followed the same order: C > C-F > C-F-C > F-C > F. A higher k_1 meant a greater tendency for MPs to attach to the sand surface initially, while a higher k_{1d} facilitated the release of attached MPs back into solution. Consequently, the dynamic attachment-release process allowed more MPs to pass through the sand column, contributing to the higher C/C_0 and M_{eff}. For sites conceptualized as irreversible (Site 2), the attachment coefficient (k_2) followed the opposite order: F > F-C > C-F-C > C-F > C. A lower k_2 indicated a weaker tendency for long-term trapping, also allowing for more MPs to be transported to the outlet, resulting in higher transport efficiency.

Therefore, the observed trends in MP transport can be explained by the combined effects of reversible deposition dynamics (governed by k_1 and k_{1d}), irreversible trapping (governed by k_2), and the specific layer configurations. For instance, the C structure exhibited the fastest and highest MP breakthrough due to its highest k_1 and k_{1d} values, lowest k_2 value, highest permeability (resulting in enhanced flow velocity), and most reduced specific surface area (limited deposition sites) [13]. In the

layered structures, the position of the low-permeability fine sand layer (with high specific surface area providing more deposition sites) in the 10-cm column played an important role. Specifically, the C-F structure, with fine sand positioned closest to the inlet (the source of MPs), exhibited the highest BTCs among the layered structures. Conversely, the F-C structure, with fine sand farthest from the inlet, exhibited the lowest layered BTCs, while the C-F-C structure showed intermediate behavior. This highlighted that MP transport was governed by both deposition kinetics and the physical architecture of the porous media, with the sequence of layers being a critical factor modulating breakthrough.

Complementary to the effluent data, the total mass percentages of MPs retained within the sand column (M_{ret}) across different structures (Cases 1–5) (Table S2) followed the order of F > F-C > C-F-C > C-F > C. This order was opposite to that observed for *MEC* and M_{eff}. Consistent with the effluent results, among the layered structures, the F-C structure exhibited the strongest ability to retain MPs, while the C-F structure exhibited the weakest. Fig. 2b shows the retention profiles (RPs) along the depth of the columns for the different structures, with layered interfaces indicated by dashed lines. In the single-layer structures, retention in each sand slice was much higher in the F structure than in the C structure. This was attributed to the lower permeability of the F structure, which impeded the transport of MPs through the column, and its higher specific surface area, which provided more deposition sites. In the layered structures, the spatial distribution of retained MPs along the column height showed greater variation (*i.e.*, more pronounced peaks and troughs) compared to the relatively uniform distributions in the single-layer C and F structures. Furthermore, in all layered structures, the retention of MPs in the fine sand layers was significantly higher than that in the coarse sand layers. This observation was confirmed by SEM images of the C-F-C structure (Fig. S4), which revealed much denser deposition of MPs on the fine sand compared to the coarse sand.

As demonstrated by the results of BTCs and RPs, the characteristics of the sand layers, including grain size, specific surface area, and permeability coefficient, played a crucial role in the deposition, transport, and retention of MPs. However, the application of classical DLVO theory, which relies on volume-averaged physicochemical properties (*e.g.*, mean zeta potential) (**Text S3**), failed to distinguish between the three layered structures, as evidenced by their overlapping interaction energy curves (Fig. S6). This failure occurred because the averaging approach inherently disregarded the specific spatial configuration of the sand layers, which profoundly impacts local pore-scale hydrodynamics and particle transport paths. Consequently, although the averaged DLVO profiles for the layered structures fell between the two end-members (single-layer C and F), partially aligning with the intermediate breakthrough behavior, the theory was fundamentally unable to capture the distinct transport behaviors observed for each unique layered sequence. This discrepancy between theory and experiment serves a diagnostic purpose, highlighting the fundamental limitations of classical DLVO theory in heterogeneous porous media, stemming from its homogenization of surface properties, idealized geometry, and neglect of hydrodynamic coupling. Therefore, accurately predicting MP transport in layered systems requires models that integrate pore-scale geometry, spatial chemical heterogeneity, and fluid dynamics.

Given that the C-F structure exhibited the highest mobility and thus the highest potential for MP diffusion and contamination among the layered structures, the effects of different solution chemistry properties (ionic strength, cation valence, and pH) on MP transport were specifically investigated using the C-F structure in the subsequent analysis.

3.2. Influence of solution chemistry on the transport of MPs in the C-F layered structure

3.2.1. Effects of ionic strength

Fig. 3 compares the impact of different ionic strengths (IS, adjusted using Na^+ solutions at 1, 10, and 30 mM) on the transport and retention of MPs in the C-F layered structure. Both the BTCs and RPs demonstrated IS-dependent patterns. As shown in Fig. 3a, the transport efficiency of MPs, reflected by the C/C_0 values in the BTCs, decreased with increasing IS. The maximum C/C_0 was significantly higher for 1 mM Na^+ case than for 10 mM Na^+, and slightly higher for 10 mM Na^+ case than for 30 mM Na^+. This non-linear decrease in C/C_0 suggested that the hindrance effect of increasing IS on MP transport did not scale linearly. Complementary quantitative metrics derived from the column experiments (Table S2) support this observation: among the three IS cases of Na^+ solutions, *MEC* and M_{eff} were highest at 1 mM IS (0.561 and 51.4 %, respectively), and lowest at 30 mM IS (0.427 and 37.6 %). Additionally, the reduction in both *MEC* and M_{eff} between 10 mM and 30 mM IS was notably smaller than the reduction between 1 mM and 10 mM IS, further indicating a diminishing inhibitory effect at higher IS. Conversely, the values of M_{ret} followed the order: 30 mM Na^+ > 10 mM Na^+ > 1 mM Na^+. This confirmed that the amount of MPs trapped within the C-F structure increased with IS, with the 30 mM Na^+ case exhibiting the strongest retention capacity and the 1 mM Na^+ case the weakest. Fig. 3b illustrates how increasing IS enhanced MP retention within both the coarse and fine sand layers of the C-F structure. While retention increased in both layers with IS, the fine sand layer consistently exhibited higher retention capacity than the coarse sand layer across all IS conditions. This difference can be attributed to the inherent physical properties of the fine sand, including its smaller grain size, larger specific surface area, and lower permeability, which favor particle capture via physical straining and potentially offer more deposition sites.

The observed inverse correlation between MP transport efficiency and IS, and the corresponding direct correlation between retention capacity and IS, can be systematically explained through deposition kinetics (Table S2), particle characteristics (Table S1), and interparticle interaction energy profiles (Fig. 4). Analysis of the two-site retention model revealed distinct IS dependencies of the two types of deposition sites. For reversible deposition sites (Site 1), both k_1 and k_{1d} decreased with increasing IS, following the order: 1 mM Na^+ > 10 mM Na^+ > 30 mM Na^+ (Table S2). The higher k_1 and k_{1d} values at low IS (1 mM) indicated a more dynamic attachment-release process. This dynamic process enabled more MPs to be transiently captured and subsequently released, enabling a larger fraction to ultimately escape retention and reach the column outlet, contributing to the higher C/C_0 and M_{eff}. In contrast, for kinetically less reversible sites (Site 2), k_2 increased with IS (30 mM Na^+ > 10 mM Na^+ > 1 mM Na^+). Consequently, at higher IS, a larger fraction of MPs encountering these sites become more

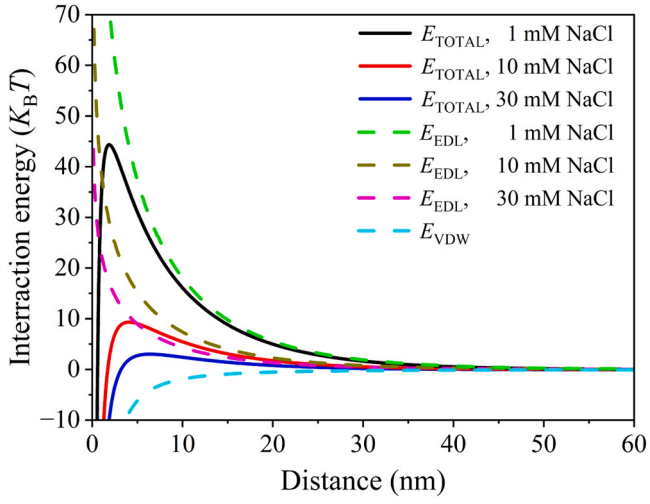

Fig. 4. Total interaction energy (E_{TOTAL}), electrostatic double layer repulsive energy (E_{EDL}), and van der Waals attraction energy (E_{VDW}) between MPs and sand particles in Na^+ solutions with varying ionic strengths (1 mM, 10 mM, and 30 mM).

permanently retained under the given experimental flow conditions, further reducing transport efficiency.

The primary underlying physical-chemical mechanism involves the compression of the electrical double layer surrounding both the MPs and the sand media surfaces as Na^+ concentration increases. This compression significantly reduced the magnitude (absolute value) of the zeta potentials: MPs shifted from −16.90 mV (1 mM) to −5.18 mV (30 mM) and sand media shifted from −4.59 mV to −3.58 mV (Table S1). The diminished surface charge reduced the electrostatic double layer repulsive energy between particles, resulting in a corresponding 93 % decrease in the repulsive energy barrier from 44.3 K_BT to 3.1 K_BT (Fig. 4). This collapse of the repulsive barrier allowed the van der Waals attraction forces to dominate, and eventually facilitated the deposition of MPs onto the sand grains. Additionally, the reduced electrostatic repulsion at higher IS also facilitated MP aggregation via charge neutralization. This resulted in 35 % increase in the average hydrodynamic diameter of the MPs, from 367.5 nm (1 mM) to 497.0 nm (30 mM) (Table S1). These enlarged particles experienced reduced accessibility within the pore spaces of the porous media, thereby enhancing the likelihood of physical straining, particularly in the finer sand layers. Furthermore, the relatively small differences observed in the BTCs, *MEC*, and M_{eff} between the 10 mM and 30 mM IS cases (compared to the larger difference between 1 mM and 10 mM) were consistent with the smaller changes in zeta potentials, hydrodynamic diameters, and the resultant total interaction energy profiles over this IS range (Table S1, and Fig. 4).

3.2.2. *Effects of cation valence*

Fig. 5 compares the impact of cation valence (Na^+ *vs.* Mg^{2+}) on the transport and retention of MPs in the C-F structure under controlled total IS conditions (1 mM and 30 mM). As shown in Fig. 5a, at 1 mM IS, the normalized effluent concentration (C/C_0) was relatively higher for Na^+ than Mg^{2+}, indicating stronger transport retardation by divalent cations. At 30 mM IS, their BTCs almost overlapped, suggesting that the hindrance effect of Mg^{2+} on MP transport in the C-F structure relative to Na^+ weakened at high IS. Supporting this trend, Table S2 shows that *MEC* and M_{eff} were highest for Na^+, 1 mM IS (Case 3) at 0.561 and 51.4 %, respectively, while the values of *MEC* and M_{eff} for Mg^{2+}, 1 mM IS were considerably lower (Case 8) than in Case 3. At 30 mM IS, the values of *MEC* and M_{eff} were similar for both cations, and much smaller than cases at 1 mM IS. The values of M_{ret} followed the order: Mg^{2+}, 30 mM IS (Case 9) > Na^+, 30 mM IS (Case 7) > Mg^{2+}, 1 mM IS (Case 8) > Na^+, 1 mM IS (Case 3). This indicated that at the same IS, Mg^{2+} exhibited higher retention than Na^+. Despite the convergent transport at 30 mM IS, Mg^{2+} had the strongest ability to retain MPs in the sand column, while Na^+ at 1 mM IS exhibited the weakest. As shown in Fig. 5b, fine sand retained more MPs than coarse sand across all conditions, attributed to its higher surface area and smaller pore throats.

The observed inverse correlation between MP transport efficiency and cation valence at identical IS arises from valence-dependent interfacial interactions, as evidenced by deposition kinetics (Table S2), particle characteristics (Table S1), and interaction energy profiles (Fig. 6). Analysis of the two-site retention model revealed distinct valence dependencies for reversible (Site 1) and kinetically less reversible (Site 2, conceptualized as irreversible) deposition sites. For reversible deposition sites (Site 1), both k_1 and k_{1d} decreased with increasing valence, following the order: Na^+, 1 mM IS > Mg^{2+}, 1 mM IS > Na^+, 30 mM IS> Mg^{2+}, 30 mM IS (Table S2). Compared to Mg^{2+} at identical IS, the higher k_1 and k_{1d} values in the Na^+ systems indicated a more dynamic attachment-release process at the reversible sites. This dynamic process enabled more MPs to be transiently captured and subsequently released, enabling a larger fraction to ultimately escape retention and reach the column outlet, contributing to the higher C/C_0 and M_{eff}. In contrast, for irreversible deposition sites (Site 2), k_2 increased with valence at identical IS: Mg^{2+}, 30 mM IS > Na^+, 30 mM IS > Mg^{2+}, 1 mM IS > Na^+, 1 mM IS. Consequently, at higher cation valence, a larger fraction of MPs

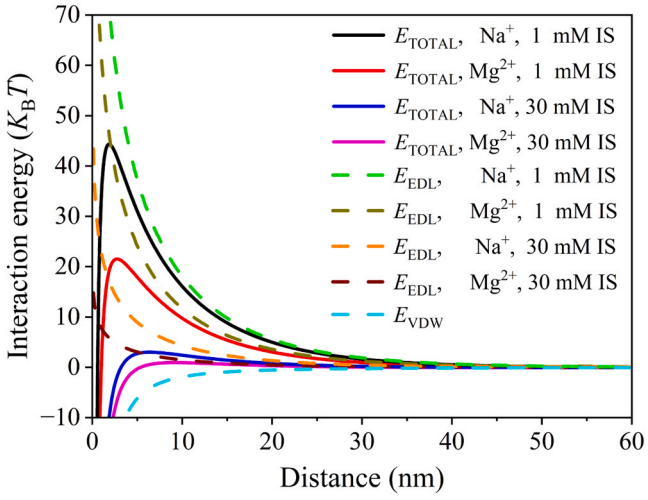

Fig. 6. Total interaction energy (E_{TOTAL}), electrostatic double layer repulsive energy (E_{EDL}), and van der Waals attraction energy (E_{VDW}) between MPs and sand for different cation valence (Na^+, Mg^{2+}) at controlled IS (1 mM and 30 mM).

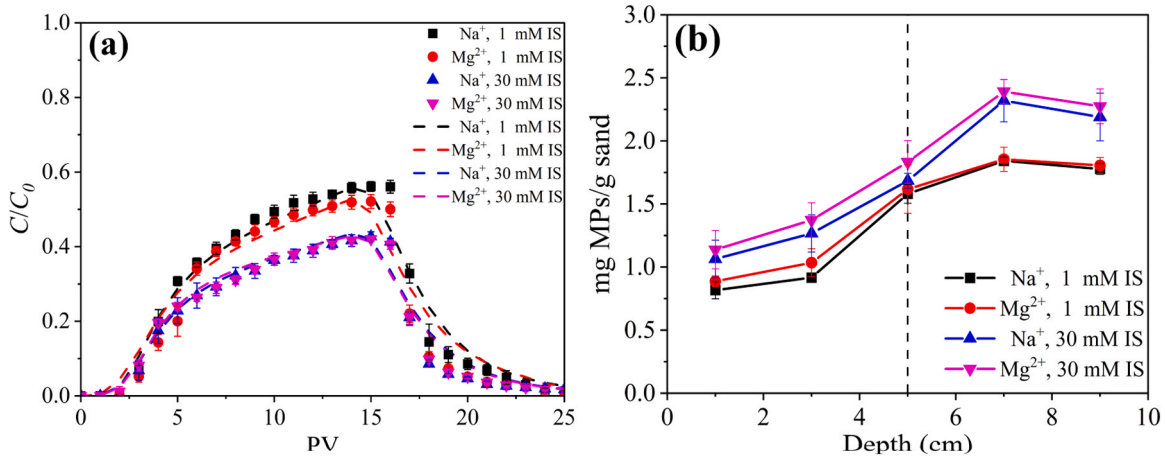

Fig. 5. Impact of cation valence (Na^+ *vs.* Mg^{2+}) on transport and retention of MPs under controlled IS (1 mM and 30 mM): (a) breakthrough curves (symbols: experimental data; dashed lines: fitting curves); (b) retention profiles (black dashed line: layered interface for the C-F structure).

encountering these sites become more permanently retained via stronger attachment, further reducing transport efficiency.

The primary underlying physical-chemical mechanism involves the compression of the electrical double layer surrounding both the MPs and the sand media surfaces as cation valence increases. This compression significantly reduced the magnitude (absolute value) of the zeta potentials: at 1 mM IS, MPs shifted from −16.90 mV (Na^+) to −11.16 mV (Mg^{2+}) and sand media shifted from −4.59 mV to −4.50 mV; at 30 mM IS, MPs shifted from −5.18 mV (Na^+) to −4.43 mV (Mg^{2+}) and sand media shifted from −3.58 mV to −2.75 mV (Table S1). The diminished surface charge reduced the electrostatic double layer repulsive energy between particles, resulting in a corresponding 52 % decrease in the repulsive energy barrier from 44.3 K_BT to 21.5 K_BT (Case 3 and 8), and a 71 % decrease in the repulsive energy barrier from 3.1 K_BT to 0.9 K_BT (Case 7 and 9) (Fig. 6). This collapse of the repulsive barrier allowed the van der Waals attraction forces to dominate, and eventually facilitated the deposition of MPs onto the sand grains. Additionally, the reduced electrostatic repulsion at higher cation valence also facilitated MP aggregation via charge neutralization. This resulted in a 5 % increase in the average hydrodynamic diameter of the MPs at 1 mM IS, from 367.5 nm (Na^+) to 385.5 nm (Mg^{2+}), and a 13 % increase at 30 mM IS (Table S1). These enlarged particles might experience reduced accessibility within the pore spaces of the porous media, thereby enhancing the likelihood of physical straining, particularly in the finer sand layers.

3.2.3. *Effects of pH*

Fig. 7 compares the impact of different pH values (5, 7, and 9) on the transport and retention of MPs in the C-F structure. As shown in Fig. 7a, the transport efficiency of MPs in porous media increased with increasing pH value. The C/C_0 value which reflected transport efficiency was highest at pH= 9 (Case 11) and lowest at pH= 5 (Case 10). As shown in Table S2, among the three pH cases, *MEC* and M_{eff} were highest in the pH= 9 case at 0.647 and 56.2 %, respectively, and lowest in the pH= 5 case at 0.505 and 44.2 %. These data collectively indicated that MPs displayed the highest mobility at pH= 9 and lowest at pH= 5, with the pH= 7 condition positioned as an intermediate state. In terms of the retention efficiency, the order of M_{ret} was pH= 5 > pH= 7 > pH= 9, indicating that the retained amounts of MPs correspondingly decreased with increasing pH value. Specifically, the pH= 5 case had the strongest ability to retain MPs in the sand column, while the pH= 9 case exhibited the weakest. As shown in Fig. 7b, an increase in pH weakened the retention of MPs in both the coarse and fine sand layers of the C-F structure. Although both sand layers experienced a pH-induced reduction in retention capacity, the fine sand layer consistently demonstrated superior retention performance compared to the coarse sand. This can be attributed to the inherent physical properties of the fine sand layer, including its smaller grain size, larger surface area, and lower permeability.

The observed direct correlation between MP transport efficiency and pH, and the inverse correlation between retention capacity and pH arises from pH-dependent interfacial interactions, as evidenced by attachment kinetics (Table S2), particle characteristics (Table S1), and interaction energy profiles (Fig. 8). Analysis of the two-site retention model revealed distinct pH dependencies for reversible (Site 1) and kinetically less reversible (Site 2, conceptualized as irreversible) sites. For reversible sites (Site 1), both k_1 and k_{1d} increased with pH (Table S2), indicating a more dynamic attachment-release process at the reversible sites at higher pH value. This dynamic process enabled more MPs to be transiently captured and subsequently released, enabling a larger fraction to ultimately escape retention and reach the column outlet, contributing to the higher C/C_0 and M_{eff}. In contrast, for irreversible sites (Site 2), k_2 decreased with pH. Consequently, the reduced long-term retention via attachment at high pH further enhanced transport efficiency.

As pH increased from 5 to 9, the deprotonation of functional groups would increase the negative charge density on MPs. The zeta potentials of MPs became more negative, from −15.20 mV to −17.00 mV

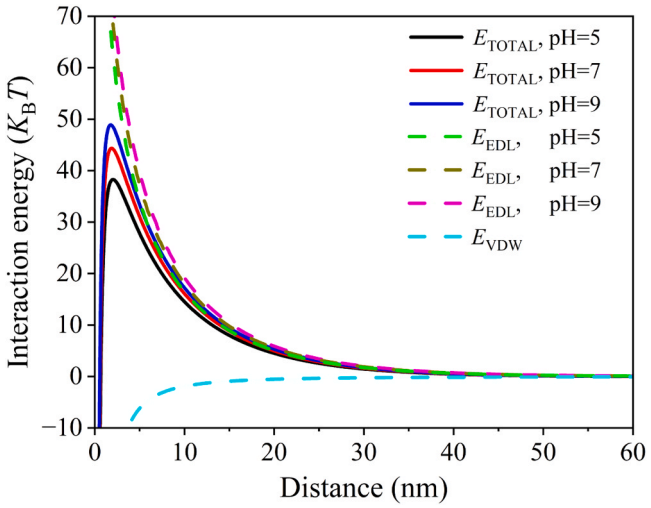

Fig. 8. Total interaction energy (E_{TOTAL}), electrostatic double layer repulsive energy (E_{EDL}), and van der Waals attraction energy (E_{VDW}) between MPs and sand under different pH conditions (5, 7, and 9).

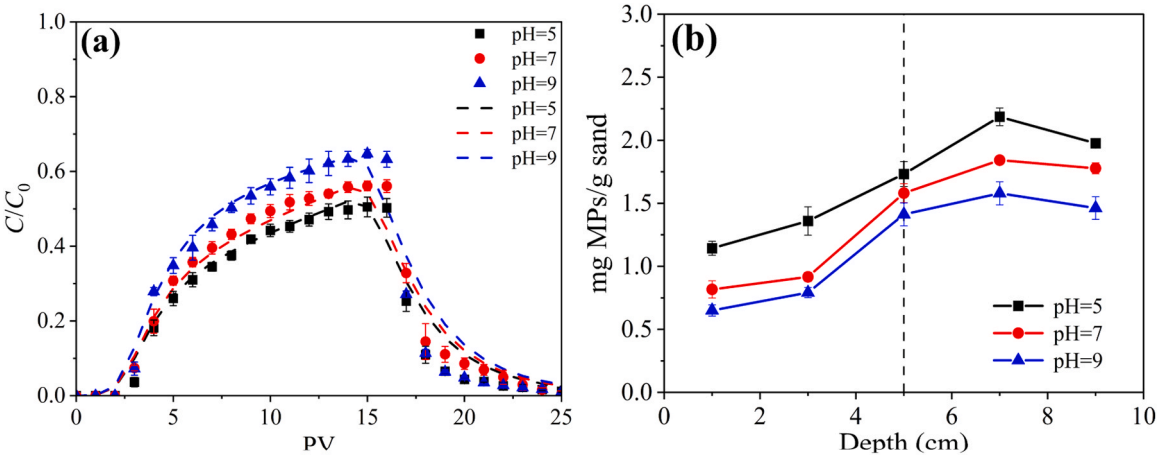

Fig. 7. Impact of different pH values (5, 7, and 9) on transport and retention of MPs: **(a)** breakthrough curves (symbols: experimental data; dashed lines: fitting curves); **(b)** retention profiles (black dashed line: layered interface for C-F structure).

(Table S1). This increased charge density reduced the effect of charge screening, enhanced the electrostatic repulsion between MPs and the porous medium [28]. The repulsive energy barrier increased by 28 %, from 38.2 K_BT to 48.9 K_BT (Fig. 8). The higher energy barrier promoted the dominant role of the electrostatic double layer interaction, inhibiting deposition and eventually facilitating transport of MPs. Additionally, the enhanced interparticle repulsion suppressed MP aggregation, decreasing their hydrodynamic diameters by 34 % (from 549.5 nm at pH=5–362.5 nm at pH=9). This decrease in particle size increased the accessibility of the MPs within the porous media, thereby diminishing the likelihood of physical straining and further promoting transport.

3.3. Discussion

We designed a series of experiments and simulations to address the gap in understanding how varying layered structures and the solution chemistry properties affect the transport and retention of MPs. However, our study had several limitations that should be acknowledged. First, although the use of small one-dimensional columns allowed controlled and repeatable isolation of key variables (e.g., sand layer sequence, solution chemistry), it could not fully represent the three-dimensional complexities of real-world scenarios. The narrow diameter limits the inclusion of lateral heterogeneity, while the short height may not adequately capture vertical stratification and hydrological dynamics. Although such one-dimensional investigations are valuable for abstracting key controlling variables from complex natural environments, clarifying mechanisms, and quantifying effects under repeatable and controlled conditions [29], they cannot fully reflect the spatial heterogeneity and hydrological complexity of actual soil systems. Future research should therefore employ multidimensional experimental setups and larger-scale models to verify and scale up our findings, enhancing their practical relevance in natural environments. Second, the artificial sand filling method used in the experiments resulted in a non-uniform compaction degree of the sand. This potential heterogeneity in packing likely introduced additional variability into the experimental results, which represents a source of uncertainty when comparing experimental and simulated breakthrough curves. Furthermore, to better align with natural subsurface conditions, no physical demarcations were used at layer interfaces, avoiding the creation of artificially sharp boundaries. Future studies should combine experimental systems with controlled gradational interfaces and modeling approaches (e.g., pore-network models) to further elucidate how interface properties modulate MP transport dynamics. Third, in actual MP-contaminated sites, factors such as temperature, microbial degradation, and soil geochemical reaction can also significantly affect the transport of MPs [30–32]. These factors were not incorporated into our study and warrant further investigation.

Fourth, the PS particles used in this study are model colloids and thus simpler than the complex heterogeneous MPs found in nature. However, our goal was not to replicate environmental complexity but to establish a mechanistic baseline for MP transport under controlled conditions. Using well-characterized PS particles allows us to isolate key variables (e.g., sand layer sequence) without interference from the irregular shapes and heterogeneous surfaces of environmental MPs. The resulting data provide a quantitative reference for future studies investigating how plastic-specific properties (e.g., shape irregularity, surface oxidation from environmental aging) alter transport behavior. The baseline established in this study thus enables future work to better distinguish whether observed effects are due to plastic aging and morphology, or due to fundamental transport mechanisms. Fifth, the mathematical model used in our study, while effective for simulating solute and colloid transport, did not explicitly account for aggregation dynamics, which is a key mechanism for nanoparticle transport and can be important for MPs under specific conditions (e.g., high salinity or smaller particle sizes) [33–35]. However, for the 1 μm MPs under the low-salinity conditions (up to 30 mM NaCl) examined in this study, aggregation is not expected to be the dominant retention mechanism. As demonstrated by Dong et al. [36], MPs in the size range of 0.8–1.5 μm exhibited negligible aggregation in low-salinity environments (e.g., 3.5 PSU, ~60 mM NaCl). Nevertheless, future work involving smaller nanoparticles or higher salinities would benefit from the integration of advanced modeling approaches that incorporate population balance equations for aggregation [34,35]. Lastly, our investigations of different solution chemistry properties were confined to the C-F structure. Future research could expand this scope to provide a more comprehensive understanding of the combined effects of solution chemistry and layered structures across different systems.

Nevertheless, our study highlighted the significance of different sequences of fine and coarse sand layer, the permeability of each layer, and the position of the leakage source in the layered soil system, on the transport and retention of MPs. These findings could provide guidance for controlling the spread of MPs and minimizing their impact on the environment. The fine sand, with its smaller pore size, enhances the retention of MPs through attachment. Additionally, its larger specific surface provides more deposition sites for MPs, further promoting their retention. Permeability is closely related to the flow velocity of the fluid in the soil. Layers with low permeability, like fine sand, tend to slow down the flow velocity. As a result, the transport of MPs is impeded, and they are more likely to be retained in such low-permeability layers. The position of the leakage source in the layered soil system also significantly influences the transport and retention of MPs. In our study, for the C-F structure where fine sand was closest to the inlet (leakage source of MPs), MPs were immediately introduced into a low-permeability environment. The smaller pore spaces and high specific surface area in the fine sand enhanced the retention of MPs through deposition and attachment. However, despite the retention capacity, the continuous injection of MPs led to a higher concentration near the inlet, resulting in higher BTCs.

While it is acknowledged that solution chemistry modulates the breakthrough behavior of MPs, our systematic experiments of varying ionic strength, cation type, and pH provided a critical insight: although these chemical changes significantly altered the absolute retention of MPs, the substantially higher retention in the fine sand layer remained robust and dominant across all tested conditions. This persistent pattern underscores that the physical architecture of the porous media sets the fundamental stage for MP transport. The chemical modulation we observed is mechanistically explained by the classic DLVO theory of colloid stability. Increased ionic strength and the presence of divalent cations like Mg^{2+} compressed the electrical double layer around both MPs and sand grains. This reduced the electrostatic repulsion, thereby lowering the energy barrier for attachment and allowing van der Waals attraction to dominate. Consequently, the attachment of MPs onto sand surfaces was enhanced. Conversely, higher pH strengthened the negative zeta potential of MPs (Table S1), amplifying electrostatic repulsion and thus promoting MP transport. In essence, solution chemistry governs the attachment efficiency by altering the net interaction energy between MPs and sand grains.

This dominant grain-size effect, however, cannot be explained by physical straining. Pore throat diameters were estimated based on a geometric relationship for granular media [37], yielding ranges of 76–150 μm for coarse sand) and 15–46 μm for fine sand. Crucially, these values, representing conservative estimates of the smallest pore throats, were one to two orders of magnitude larger than the hydrodynamic diameter of the MPs (362.5–549.5 nm, Table S1). This vast disparity rules out straining as a significant retention mechanism in the bulk porous media. Furthermore, zeta potential measurements (Table S1) confirmed that the sand grains exhibited a consistent negative charge under equivalent conditions (e.g., approximately −4.5 mV at low IS, −2.75 mV in 30 mM $MgCl_2$), verifying the effectiveness of our cleaning protocol. MPs also exhibited distinct charge variations, becoming less negative with increasing ionic strength/Mg^{2+} and more negative with increasing pH. Notably, even with these charge modulations, the relative retention pattern (fine sand > coarse sand) remained unaffected,

confirming that physical structure dominates the overall retention pattern, while solution chemistry modulates the efficiency of attachment within that structure.

Therefore, MP retention emerges as a synergistic process. The physical architecture, e.g., larger specific surface area providing more deposition sites and greater flow resistance in fine sand increasing contact time, primarily determines the frequency and duration of MP-sand collisions. In contrast, the solution chemistry dictates the probability of a collision resulting in successful attachment. The inability of chemical conditions to override the layer sequence effect demonstrates that the physical framework is the primary determinant of retention patterns, while chemistry acts as a powerful modulator within that fixed framework. The potential formation of a filter cake layer was also considered [38]. However, the stable hydraulic conductivity throughout our experiments suggests it was not a dominant mechanism under the specific conditions of low MP concentration and upward flow. This further supports the conclusion that attachment within the sand matrix itself was the primary retention mechanism. Nonetheless, in scenarios with higher particle loading, the filter cake effect could become significant and warrants future investigation.

4. Conclusions

This study demonstrated that the transport and retention of microplastics (MPs) in saturated porous media are governed by a complex interplay between layered physical structures and solution chemistry. The sequence of sand layers emerged as a critical yet previously underappreciated influencing factor, with the Coarse-Fine (C-F) structure facilitating higher mobility and the Fine-Coarse (F-C) structure exhibiting effective filtration characteristics. This hierarchy in mobility was collectively determined by the confluence of deposition kinetics (higher reversible attachment/detachment coefficients and lower kinetically less reversible retention in C-F), the proximal positioning of the low-permeability and high-surface-area fine layer to the inlet in C-F, and pore-scale heterogeneity. Furthermore, while solution chemistry properties such as ionic strength, cation type, and pH modulated these transport behaviors in the C-F layered structure, i.e., enhancing mobility under conditions of lower ionic strength, monovalent cations like Na^+, and higher pH, the fundamental mechanism of preferential retention in fine-grained layers remained robust across all tested chemical conditions.

These findings underscore the need for environmental risk assessment that move beyond average media properties and explicitly incorporate stratigraphic architecture. The identification of this “layer sequence effect” provides a scientific basis for practical environmental management. It implies that under specific hydrogeological conditions, such as the presence of a natural C-F sequence coupled with favorable chemical conditions like low ionic strength and high pH, MPs pose a substantially higher risk of contamination. Consequently, for applications ranging from the siting of landfills to the design of groundwater monitoring networks, risk models must integrate detailed subsurface stratification data. Proactive mitigation strategies, such as engineering multi-layered filtration systems that leverage the contrasting hydraulic properties of different sediments to enhance MP retention, can be developed based on these insights. Ultimately, this research provides a critical foundation for predicting the fate of MPs in realistic subsurface environments and for developing targeted strategies to mitigate their environmental impact.

This study provides foundational insights, yet it is not without limitations. The laboratory-scale, one-dimensional experiments with idealized media simplify the complexity of natural field conditions. Furthermore, factors such as microbial activity and dynamic chemical gradients were not considered, and the model did not account for MP aggregation. These limitations, however, clearly outline valuable directions for future research. Future investigations should therefore focus on validating these mechanisms in more complex, field-relevant systems, with a particular emphasis on the impact of microbial processes, quantifying filtration kinetics under dynamic chemical gradients, and elucidating the potential for secondary release of retained MPs alongside their long-term transformation.

Environmental Implication

Microplastics (MPs) pose persistent threats to groundwater and soil ecosystems due to their subsurface mobility. Our study reveals that physical heterogeneity (*e.g.*, layered sequences) and chemical conditions (*e.g.*, ionic strength, cation valence, pH) jointly control MP fate in saturated porous media. Crucially, fine-grained layers persistently trap MPs, while chemical shifts (*e.g.*, seawater intrusion or alkaline rainfall) may accelerate their migration toward aquifers. These findings expose hidden contamination pathways in stratified environments, informing targeted monitoring of high-risk zones (*e.g.*, coarse-over-fine strata in our study) and optimized remediation designs to protect groundwater-dependent ecosystems.

CRediT authorship contribution statement

Didi Li: Writing – review & editing, Writing – original draft, Project administration, Funding acquisition, Conceptualization. **Yuzhe Qin:** Visualization, Validation. **Shihao Zhen:** Visualization, Validation, Investigation. **Zhimin Ao:** Writing – review & editing, Funding acquisition.

Declaration of Competing Interest

The authors declare that they have no known competing financial interests or personal relationships that could have appeared to influence the work reported in this paper.

Acknowledgements

This study was supported by the National Key R&D Program of China (Grant No. 2022YFC3901800), National Natural Science Foundation of China (Grant No. T2421005, 22176041, 41807191), the Fundamental Research Funds for the Central Universities (Grant No. 2243200011), and the Guangzhou Science and Technology Planning Project (Grant No. 2023A04J0918).

Appendix A. Supporting information

Supplementary data associated with this article can be found in the online version at doi:10.1016/j.jhazmat.2025.140502.

Data availability

Data will be made available on request.

References

[1] Law, K.L., Thompson, R.C., 2014. Microplastics in the seas. Science 345, 144–145.
[2] Sun, Y., Ding, W., Wang, Y., Zhang, Z., Wang, R., Guo, Y., Gao, Z., Du, H., Ma, D., 2025. New insight into manganese-enhanced abiotic degradation of microplastics: Processes and mechanisms. Chin Chem Lett 36, 109941.
[3] Chae, Y., An, Y.-J., 2018. Current research trends on plastic pollution and ecological impacts on the soil ecosystem: A review. Environ Pollut 240, 387–395.
[4] Ullah, R., Tsui, M.T.-K., Chow, A., Chen, H., Williams, C., Ligaba-Osena, A., 2022. Micro(nano)plastic pollution in terrestrial ecosystem: emphasis on impacts of polystyrene on soil biota, plants, animals, and humans. Environ Monit Assess 195, 252.
[5] Hou, J., Xu, X., Lan, L., Miao, L., Xu, Y., You, G., Liu, Z., 2020. Transport behavior of micro polyethylene particles in saturated quartz sand: Impacts of input concentration and physicochemical factors. Environ Pollut 263, 114499.
[6] Bläsing, M., Amelung, W., 2018. Plastics in soil: Analytical methods and possible sources. Sci Total Environ 612, 422–435.
[7] Brewer, A., Dror, I., Berkowitz, B., 2021. The Mobility of Plastic Nanoparticles in Aqueous and Soil Environments: A Critical Review. ACS EST Water 1, 48–57.

[8] Yuan, P., Cao, X., Zhao, L., Xu, X., Romero-Freire, A., Qiu, H., 2025. Overlooked yet critical pathways for microplastics input to soil and groundwater system: Transport mechanisms and simulation predictions in landfill environments. Water Res 284, 124041.
[9] Fleury, J.-B., Baulin, V.A., 2021. Microplastics destabilize lipid membranes by mechanical stretching, 118, e2104610118.
[10] Qin, X., Cao, M., Peng, T., Shan, H., Lian, W., Yu, Y., Shui, G., Li, R., 2024. Features, Potential Invasion Pathways, and Reproductive Health Risks of Microplastics Detected in Human Uterus. Environ Sci Technol 58, 10482–10493.
[11] Singer, M.N., Mohsen, B., Katzourakis, V.E., Al Shehhi, M.R., Chrysikopoulos, C.V., 2025. Mechanisms governing the transport of nanoparticles and microplastics in porous media: A review. J Environ Chem Eng 13, 118002.
[12] Fei, J., Xie, H., Zhao, Y., Zhou, X., Sun, H., Wang, N., Wang, J., Yin, X., 2022. Transport of degradable/nondegradable and aged microplastics in porous media: Effects of physicochemical factors. Sci Total Environ 851, 158099.
[13] Li, F., Huang, D., Wang, G., Cheng, M., Chen, H., Zhou, W., Xiao, R., Li, R., Du, L., Xu, W., 2024. Microplastics/nanoplastics in porous media: Key factors controlling their transport and retention behaviors. Sci Total Environ 926, 171658.
[14] Geng, C., Gao, Y., Zhang, H., Xue, D., Shan, H., Wang, B., Wang, X., Zhao, J., 2024. Microplastic migration in porous media at various scales: a review. Environ Chem Lett 22, 691–713.
[15] Sharma, V.K., Ma, X., Guo, B., Zhang, K., 2021. Environmental factors-mediated behavior of microplastics and nanoplastics in water: A review. Chemosphere 271, 129597.
[16] Wu, J., Jiang, R., Lin, W., Ouyang, G., 2019. Effect of salinity and humic acid on the aggregation and toxicity of polystyrene nanoplastics with different functional groups and charges. Environ Pollut 245, 836–843.
[17] Dong, S., Zhou, M., Su, X., Xia, J., Wang, L., Wu, H., Suakollie, E.B., Wang, D., 2022. Transport and retention patterns of fragmental microplastics in saturated and unsaturated porous media: A real-time pore-scale visualization. Water Res 214, 118195.
[18] Zhang, X., Wu, L., Han, X., Shi, Y., Huang, J., Ding, B., Zhang, Y., Zhang, Z., Shi, Y., Li, F., 2025. Effects of ionic strength, cation type and pH on the cotransport of microplastics with PFOA in saturated porous media. Chemosphere 370, 143942.
[19] Wu, X., Lyu, X., Li, Z., Gao, B., Zeng, X., Wu, J., Sun, Y., 2020. Transport of polystyrene nanoplastics in natural soils: Effect of soil properties, ionic strength and cation type. Sci Total Environ 707, 136065.
[20] Wang, X., Diao, Y., Dan, Y., Liu, F., Wang, H., Sang, W., Zhang, Y., 2022. Effects of solution chemistry and humic acid on transport and deposition of aged microplastics in unsaturated porous media. Chemosphere 309, 136658.
[21] Li, S., Yang, M., Wang, H., Jiang, Y., 2022. Adsorption of microplastics on aquifer media: Effects of the action time, initial concentration, ionic strength, ionic types and dissolved organic matter. Environ Pollut 308, 119482.
[22] Lim, S.J., Seo, J., Hwang, M., Kim, H.-C., Kim, E.-J., Lee, J., Hong, S.W., Lee, S., Chung, J., 2023. A multi-scale framework for modeling transport of microplastics during sand filtration: Bridging from pore to continuum. J Hazard Mater 443, 130219.
[23] Alimi, O.S., Farner Budarz, J., Hernandez, L.M., Tufenkji, N., 2018. Microplastics and Nanoplastics in Aquatic Environments: Aggregation, Deposition, and Enhanced Contaminant Transport. Environ Sci Technol 52, 1704–1724.
[24] Ahfir, N.-D., Hammadi, A., Alem, A., Wang, H., Bras, G.Le, Ouahbi, T., 2017. Porous media grain size distribution and hydrodynamic forces effects on transport and deposition of suspended particles. J Environ Sci 53, 161–172.
[25] Wang, Z., Li, J., Qu, Z., Ayurzana, B., Zhao, G., Li, W., 2024. Effects of microplastics on the pore structure and connectivity with different soil textures: Based on CT scanning. Environ Technol Innov 36, 103791.
[26] Dong, X., Liu, X., Hou, Q., Wang, Z., 2023. From natural environment to animal tissues: A review of microplastics(nanoplastics) translocation and hazards studies. Sci Total Environ 855, 158686.
[27] Wang, D., Zhang, W., Zhou, D., 2013. Antagonistic Effects of Humic Acid and Iron Oxyhydroxide Grain-Coating on Biochar Nanoparticle Transport in Saturated Sand. Environ Sci Technol 47, 5154–5161.
[28] Dong, S., Xia, J., Sheng, L., Wang, W., Liu, H., Gao, B., 2021. Transport characteristics of fragmental polyethylene glycol terephthalate (PET) microplastics in porous media under various chemical conditions. Chemosphere 276, 130214.
[29] Okutan, H.M., Sağir, Ç., Fontaine, C., Nauleau, B., Kurtulus, B., Le Coustumer, P., Razack, M., 2022. One-Dimensional Experimental Investigation of Polyethylene Microplastic Transport in a Homogeneous Saturated Medium, 10, 2022.
[30] An, Q., Zhen, Z., Zhong, N., Qiu, D., Xie, Y., Yan, C., 2024. Effects of biodegradable microplastics on arsenic migration and transformation in paddy soils: a comparative analysis with conventional microplastics. J Hazard Mater 469, 134053.
[31] Huo, Y., Dijkstra, F.A., Possell, M., Singh, B., 2024. Mineralisation and priming effects of a biodegradable plastic mulch film in soils: Influence of soil type, temperature and plastic particle size. Soil Biol Biochem 189, 109257.
[32] Ye, H., Li, Q., Li, J., Li, D., Ao, Z., 2025. Review on the abiotic degradation of biodegradable plastic poly(butylene adipate-terephthalate): Mechanisms and main factors of the degradation. Chin Chem Lett 36, 109861.
[33] Katzourakis, V.E., Chrysikopoulos, C.V., 2023. Investigating the effects of initial concentration and population distribution on the transport of aggregating nanoparticles in porous media. Adv Water Resour 178, 104475.
[34] Katzourakis, V.E., Chrysikopoulos, C.V., 2024. Aggregating nanoparticle transport with nonlinear attachment: Modeling and experimental validation. Adv Water Resour 193, 104819.
[35] Katzourakis, V.E., Chrysikopoulos, C.V., 2024. Advanced Mathematical Model for the Transport of Aggregating Nanoparticles in Water Saturated Porous Media: Nonlinear Attachment and Particle Size-Dependent Dispersion. Water Resour Res 60 e2024WR037056.
[36] Dong, Z., Qiu, Y., Zhang, W., Yang, Z., Wei, L., 2018. Size-dependent transport and retention of micron-sized plastic spheres in natural sand saturated with seawater. Water Res 143, 518–526.
[37] Wu, C.-H., Sharma, M.M., 2017. A DEM-based approach for evaluating the pore throat size distribution of a filter medium. Powder Technol 322, 159–167.
[38] Enfrin, M., Lee, J., Le-Clech, P., Dumée, L.F., 2020. Kinetic and mechanistic aspects of ultrafiltration membrane fouling by nano- and microplastics. J Membr Sci 601, 117890.